Journal of the Mechanics and Physics of Solids 70 (2014) 297–313

Contents lists available at ScienceDirect

Journal of the Mechanics and Physics of Solids

journal homepage: www.elsevier.com/locate/jmps

# Generalized shear of a soft rectangular block

Dong Wang, M.S. Wu *

*School of Mechanical and Aerospace Engineering, Nanyang Technological University, Singapore 639798*

ARTICLE INFO

*Article history:*
Received 6 February 2014
Received in revised form
9 June 2014
Accepted 11 June 2014
Available online 18 June 2014

*Keywords:*
Soft block
Generalized shear
Negative normal stress
Sinusoidal shear stress
Poynting effect

ABSTRACT

The problem of the simple shear of a block has been treated in terms of a shear displacement, applied uniformly in a lateral direction and assumed to be a linear function of the height above the base. In this paper, simple shear is generalized: the shear displacement is neither uniform in the lateral direction nor necessarily a linear function of the height. Using second-order isotropic elasticity, the analytical solutions show that the shear displacements are characterized by the product of sine and hyperbolic sine functions of the height and depth variables, respectively. The height dependence of the shear displacement is predicted to be a combination of linear and sinusoidal functions, and is verified against the test data of agar–gelatin cuboidal blocks. If the gravity effect is incorporated, a quadratic dependence on height is additionally predicted. The calculation of stresses reveals the presence of not only negative normal stresses but also sinusoidally varying shear stresses on the lateral planes tending to distort the block about the height direction. These results can be of great importance in tissue/cell mechanics.



## 1. Introduction

In nonlinear elasticity, the existence of normal stresses under simple shear has long been recognized (Rivlin, 1948) and so has the lengthening of a cylinder under pure torsion (Poynting, 1909). There has been a recent interest in the shearing and torsion of soft materials such as biopolymers and hydrogels, e.g., Storm et al. (2005), Janmey et al. (2007), Kang et al. (2009), Wu and Kirchner (2010), Destrade and Saccomandi (2010), Destrade et al. (2012), Mihai and Goriely (2011, 2013), and Horgan and Murphy (2011). A significant finding of some of these works is the existence of negative normal stresses or the negative Poynting effect when certain soft solids are subjected to shear or torsion. Negative normal stresses occur if the sheared faces of a block are drawn together under shear, and equivalently the negative Poynting effect occurs if a cylindrical rod shortens under torsion. The shearing of soft biological materials is common in their physiological environments (Horgan and Murphy, 2011), and understanding of nonlinear phenomena such as the Poynting effect is of great importance. For instance, the large stresses generated by the Poynting effect can result in a significant effect on the overall force balance in the cytoskeleton under shear (Janmey et al., 2007), and the Poynting effect is important in understanding the interaction between surgical instruments and tissues (Misra et al., 2010). In this paper, the simple shear problem will be generalized and investigated in some detail.

In the strain formulation of the simple shear problem, e.g., Rivlin (1948), the starting point is the deformation of a block as given by:

$$x = X + \kappa Y, \quad y = Y, \quad z = Z \tag{1.1}$$

* Corresponding author. Tel.: +65 6790 5545.
*E-mail address:* mmswu@ntu.edu.sg (M.S. Wu).

http://dx.doi.org/10.1016/j.jmps.2014.06.003
0022-5096/

where $(X, Y, Z)$ and $(x, y, z)$ are the referential and current Cartesian coordinates respectively, and $\kappa$ is the shear deformation. Murnaghan (1951) also started from Eq. (1.1) in studying simple shear within the framework of second-order elasticity. Calculation of the stresses then reveals that normal stresses must exist to support such a deformation. Recently, Destrade et al. (2012) pursued a stress formulation for hyperelastic materials in which the starting point is a uniform shear stress $\sigma_{12}=\sigma_{21}$. The resulting deformation is given by:

$$x=\lambda_1 X+\lambda_2\sqrt{1-\lambda_1{}^2\lambda_2{}^{-2}}Y,\quad y=\lambda_2 Y,\quad z=\lambda_3 Z, \tag{1.2}$$

where $\lambda_1, \lambda_2,$ and $\lambda_3$ are the principal stretches. This means that under a pure shear stress the deformation consists of a simple shear of the type given by Eq. (1.1) and triaxial extensions. Hence, under the strain formulation the resulting stress field consists of shear stresses and triaxial normal stresses, while under the stress formulation the resulting deformation field consists of simple shear and triaxial stretches. Mihai and Goriely (2013) considered generalized shear in which Eq. (1.1) is modified into:

$$x=X+\kappa(Y),\quad y=Y,\quad z=Z, \tag{1.3}$$

where $\kappa$ is now a function of $Y$. Specifically, $\kappa(Y)$ is assumed to be of the form of $Y^2/2$, i.e., a quadratic function of $Y$. Destrade and Saccomandi (2010) also considered the effect of gravity in the form of a body force $-\rho_0 g$ ($\rho_0$ is the mass density and $g$ is the gravitational constant). They took the deformation to be:

$$x=X+u(Y),\quad y=Y+v(Y),\quad z=Z, \tag{1.4}$$

where, upon solving the governing equations and assuming the Murnaghan strain energy density, $u(Y)$ was found to be the sum of linear and quadratic parts.

In this paper, we consider the generalized shear of a block with the $X$-axis as the shearing direction, the $Y$-axis the vertical direction and the $Z$-axis the depth direction. The deformation is taken to be

$$x=X+u(Y,Z),\quad y=Y+v(Y),\quad z=Z, \tag{1.5}$$

where the specific form for $u(Y, Z)$, under various prescribed displacement profiles at the top of the block, is solved from the governing equilibrium equations. Two new features of the formulation are noted: $u(Y, Z)$ is not assumed *a priori* and it could be a function of $Z$. The prescribed displacements considered are constant, quadratic and sinusoidal functions of $Z$. The dependence of $u$ on $Y$, i.e., the deformed block shows a curved rather than straight lateral profile, has been noted by Gardiner and Weiss (2001) during their finite element simulation of the simple shear of soft tissues. The form of this dependence has been assumed to be quadratic in Eq. (1.3), and predicted to be the sum of linear and quadratic terms in the gravity formulation of Eq. (1.4). In our work, we will show that, in the absence of gravity, $u$ is the sum of a linear function of $Y$ and a function of the product $\sin Y \times \sinh Z$, even if the prescribed displacement at the top of the block is uniform, i.e., $u(Y=L_Y, Z)$=constant, where $L_Y$ is the height of the block. Hence, a block of soft material subjected to a constant shear displacement at the top surface is curved in both the $X$–$Y$ and $X$–$Z$ planes (but not in the $Y$–$Z$ plane).

We also use the Murnaghan strain energy density as the constitutive law. The gravity effect can also be taken into account as was done previously by Destrade and Saccomandi (2010). We compare the shape of deformed blocks of agar–gelatin with the theoretical predictions. Furthermore, we explore the dependence of negative or positive normal stresses on the elastic constants. The paper is organized into five sections: introduction, formulation, numerical results, discussion and conclusions.

## 2. Second-order formulation of the generalized shear of a rectangular elastic block

### 2.1. Definition of problem

We consider a homogeneous isotropic rectangular block of dimensions $L_X$, $L_Y$ and $L_Z$ under generalized shear and gravity as shown in Fig. 1(a). In reference Cartesian coordinates $(X, Y, Z)$, the shear displacement is assumed to be $(U, V, 0)$, so that the final coordinates $(x, y, z)$ are given by $(X+U, Y+V, Z)$. Here $U=u_1(Y,Z)+ku_2(Y,Z)$denotes the shear displacement in the $X$-direction, with $u_1$ and $u_2$ representing the linear and nonlinear components, respectively. $U$ is taken to be a function of both $Y$ and $Z$, allowing for the possibility of a non-uniform (generalized) shear which might exist in a complex setting such as a physiological environment. Similarly,$V=v_1(Y)+kv_2(Y)$ denotes the displacement in the $Y$-direction resulting from gravity, with $v_1$ and $v_2$ denoting the linear and nonlinear components. However, $V$ is solely a function of $Y$ as this is the direction of gravity. If gravity is neglected, $V=0$. Note also that $k$ is a marker indicating the order of approximation of the theory. In the subsequent formulation, we retain terms up to $k^2$ for second-order theory.

Fig. 1(b) shows the possible deformed configuration of the block, which is fixed to the bottom plane $Y=0$, and subjected to prescribed displacement at the top face $Y=L_Y$. The linear part of the prescribed displacement is proportional to $Y$, and the nonlinear part is described by any $g(Z)$ which is symmetric with respect to $Z=L_Z/2$. Furthermore, we prescribe a moment $M_{xZ}$ about the $Z$-axis, which is associated with an induced out-of-plane shear.

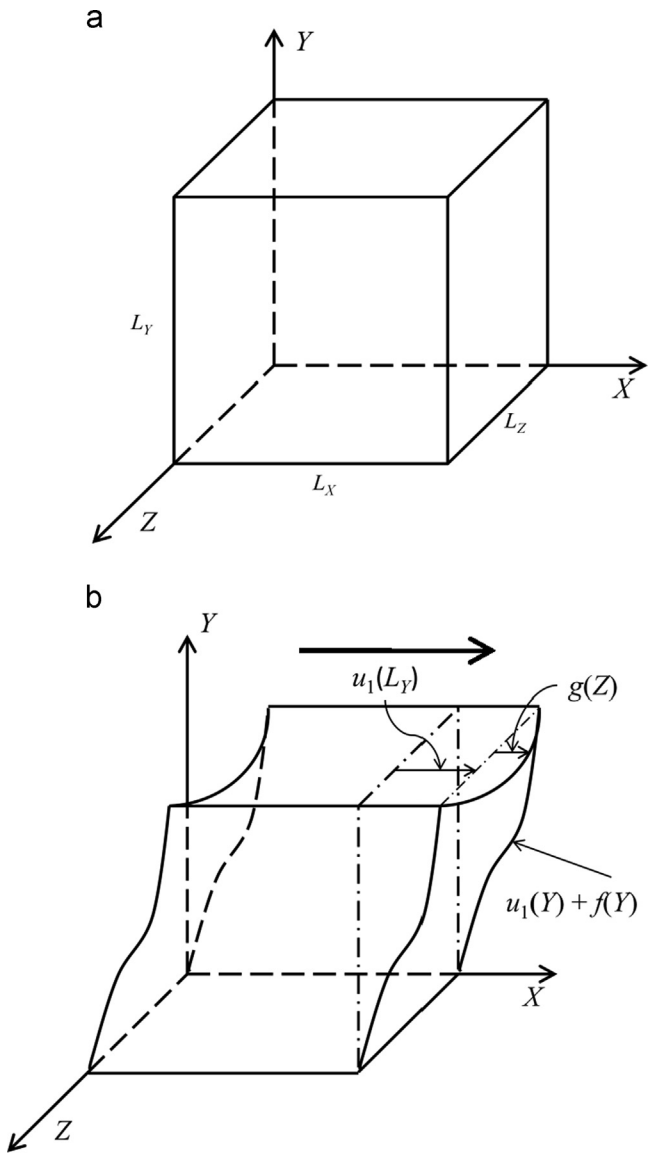


**Fig. 1.** (a) A homogeneous isotropic rectangular block of dimensions $L_X$, $L_Y$ and $L_Z$ at the undeformed state. (b) The block deformed under generalized shear. The prescribed displacement at the top face $Y=L_Y$ consists of the linear part $u_1(L_Y)$ and the nonlinear part $u_2(Y=L_Y, Z)=g(Z)$. The lateral profile of the block, or the deformed shaped of the four vertical edges of the box, can be written as $u_1(Y)+f(Y)$.

### 2.2. Governing equations

The governing equations are the equilibrium equations in the first Piola–Kirchoff stress. The stress components are expressed in terms of displacements via the second-order constitutive relations. The solutions to the governing equations are therefore displacements, the second-order parts of which are not polynomials, as will be shown in the subsections to follow. The second-order elasticity model is first briefly reviewed in Section 2.2.1, and the equilibrium equations in Section 2.2.2. The solutions in the absence of gravity are derived in Section 2.3, with particular solutions for various prescribed displacements given in Section 2.4. Finally, the solutions in the presence of gravity are listed in Section 2.5.

#### 2.2.1. Second-order elasticity model

The differentials of position vectors in the undeformed and deformed states are respectively:

$$\begin{pmatrix} dX \\ dY \\ dZ \end{pmatrix}, \quad \begin{pmatrix} dX + k\left(\frac{\partial u_1}{\partial Y}dY + \frac{\partial u_1}{\partial Z}dZ\right) + k^2\left(\frac{\partial u_2}{\partial Y}dY + \frac{\partial u_2}{\partial Z}dZ\right) \\ dY + kdv_1 + k^2 dv_2 \\ dZ \end{pmatrix}. \tag{2.1}$$

The deformation gradient **F** can then be written as:

$$\mathbf{F}=\begin{pmatrix} 1 & k\frac{\partial u_1}{\partial Y}+k^2\frac{\partial u_2}{\partial Y} & k\frac{\partial u_1}{\partial Z}+k^2\frac{\partial u_2}{\partial Z} \\ 0 & 1+k\frac{dv_1}{dY}+k^2\frac{dv_2}{dY} & 0 \\ 0 & 0 & 1 \end{pmatrix}, \tag{2.2}$$

where partial derivatives are used for $u_1$ and $u_2$. In comparison, the deformation gradient **F** in previous works (Horgan and Murphy, 2011; Gardiner and Weiss, 2001; Mihai and Goriely, 2013) take the form:

$$\mathbf{F}=\begin{pmatrix} a & \kappa & 0 \\ 0 & b & 0 \\ 0 & 0 & c \end{pmatrix}, \tag{2.3}$$

where $a$, $b$, and $c$ are constants, and $\kappa$ is a constant or a function of $y$ which represents the shear. Destrade and Saccomandi (2010) considers gravity and **F** takes the form:

$$\mathbf{F}=\begin{pmatrix} 1 & \frac{du(Y)}{dY} & 0 \\ 0 & 1+\frac{dw(Y)}{dY} & 0 \\ 0 & 0 & 1 \end{pmatrix}, \tag{2.4}$$

where $u$ and $w$ represent the shear displacement and displacement caused by gravity, respectively. In our formulation, **F** in Eq. (2.1) contains an additional term $k(\partial u_1/\partial Z)+k^2(\partial u_2/\partial Z)$, which exists because the shear displacement is a function of both $Y$ and $Z$.

The energy density $W$ of Murnaghan (1951) is

$$W=\frac{\lambda+2\mu}{2}J_1^2-2\mu J_2+\frac{l+2m}{3}J_1^3-2mJ_1J_2+nJ_3, \tag{2.5}$$

where $\lambda$ and $\mu$ are the second-order and $l$, $m$, $n$ the third-order elastic constants, respectively, and $J_1$, $J_2$, and $J_3$ are the strain invariants of the Lagrangian strain **E**:

$$J_1=E_1+E_2+E_3,\quad J_2=E_1E_2+E_2E_3+E_3E_1,\quad J_3=E_1E_2E_3. \tag{2.6}$$

The Lagrangian strain is expressed in terms of the deformation gradient as:

$$\mathbf{E}=\frac{1}{2}(\mathbf{F}^*\mathbf{F}-\mathbf{I}), \tag{2.7}$$

where **I** is the identity and the asterisk denotes the transpose. The first Piola–Kirchhoff stress (relating forces in the current configuration to area vectors in the undeformed configuration, and generally non-symmetric) is defined as

$$\mathbf{T}=\mathrm{F}\frac{\partial W}{\partial \mathbf{E}}=\mathrm{F}(\lambda J_1\mathrm{I}+2\mu\mathrm{E}+(lJ_1^2-2mJ_2)\mathrm{I}+2mJ_1\mathrm{E}+n\ co\ \mathbf{E}), \tag{2.8}$$

where co **E** is the cofactor matrix.

### 2.2.2. Equilibrium equations

The Lagrangian equilibrium equations in Cartesian coordinates can be written as

$$\begin{aligned} &\frac{\partial T_{xX}}{\partial X}+\frac{\partial T_{xY}}{\partial Y}+\frac{\partial T_{xZ}}{\partial Z}=0,\\ &\frac{\partial T_{yX}}{\partial X}+\frac{\partial T_{yY}}{\partial Y}+\frac{\partial T_{yZ}}{\partial Z}-\rho_0 g=0,\\ &\frac{\partial T_{zX}}{\partial X}+\frac{\partial T_{zY}}{\partial Y}+\frac{\partial T_{zZ}}{\partial Z}=0, \end{aligned} \tag{2.9}$$

where $\rho_0$ is the mass density in the reference configuration. The notation for the stress components is exemplified by $T_{xX}$, which means the stress acting in the $x$-direction on an element surface with $X$ as the direction of the normal vector. Tensorially, the first Piola–Kirchhoff stress $\mathbf{T}=T_{aB}\mathbf{e}_a\otimes\mathbf{E}_B$, where $T_{aB}$are the components and $\mathbf{e}_a$, $\mathbf{E}_B$are the basis vectors in the deformed and reference configurations. Substituting the stresses from Eq. (2.8) into Eq. (2.9) yields the following two first-order and three second-order equations:

$$k\mu\left(\frac{\partial^2 u_1}{\partial Y^2}+\frac{\partial^2 u_1}{\partial Z^2}\right)=0, \tag{2.10}$$

$$k^2\left(\begin{array}{l}\frac{1}{2}(2\lambda+2m-n)v_1'\frac{\partial^2 u_1}{\partial Z^2}+(\lambda+2\mu+m)v_1''\frac{\partial u_1}{\partial Y}+(\lambda+2\mu+m)v_1'\frac{\partial^2 u_1}{\partial Y^2}+\\ \mu\left(\frac{\partial^2 u_2}{\partial Y^2}+\frac{\partial^2 u_2}{\partial Z^2}\right)\end{array}\right)=0, \tag{2.11}$$

$$k((\lambda+2\mu)v_1''-g\rho_0)=0, \tag{2.12}$$

$$\begin{aligned}&\frac{1}{4}k^2((4m-n)\frac{\partial u_1}{\partial Z}\frac{\partial u_1^2}{\partial Y\,\partial Z}+4(\lambda+2\mu+m)\frac{\partial u_1}{\partial Y}\frac{\partial u_1^2}{\partial Y^2}+4(\lambda+\mu)\frac{\partial u_1}{\partial Z}\frac{\partial u_1^2}{\partial Y\,\partial Z}\\&+(4\mu+n)\frac{\partial u_1}{\partial Y}\frac{\partial u_1^2}{\partial Z^2}+4(\lambda+2\mu)v_2''+4v_1'v_2''(3\lambda+2l+6\mu+4m))=0,\end{aligned} \tag{2.13}$$

$$\frac{1}{4}k^2\left(\frac{\partial u_1}{\partial Y}\frac{\partial u_1^2}{\partial Y\,\partial Z}(4\lambda+4\mu+4m-n)+\frac{\partial u_1}{\partial Z}\left(4(\lambda+2\mu+m)\frac{\partial u_1^2}{\partial Z^2}+(4\mu+n)\frac{\partial u_1^2}{\partial Y^2}\right)\right)=0. \tag{2.14}$$

The third first-order equation, which arises from the third of Eq. (2.9), is identically zero. Also, $v_1''$ in Eq. (2.12) denotes the second-order derivative of $v_1$ with respect to $Y$. Further note that Eq. (2.10) is the Laplace equation, Eq. (2.12) is a second-order ordinary differential equation, while the remaining appear to be rather complicated partial differential equations. The displacement $u_2$ appears only in Eq. (2.11).

### 2.3. General solutions without gravity

In this section, the general solutions of a rectangular block under generalized shear without gravity are obtained. Thus, $v_1(Y)=v_2(Y)=0$ and Eqs. (2.10)–(2.14) reduce to the following four equations:

$$k\mu\left(\frac{\partial^2 u_1}{\partial Y^2}+\frac{\partial^2 u_1}{\partial Z^2}\right)=0, \tag{2.15}$$

$$k^2\mu\left(\frac{\partial^2 u_2}{\partial Y^2}+\frac{\partial^2 u_2}{\partial Z^2}\right)=0, \tag{2.16}$$

$$\frac{1}{4}k^2\left(\frac{\partial u_1}{\partial Z}\frac{\partial^2 u_1}{\partial Y\,\partial Z}(4\lambda+4\mu+4m-n)+4(\lambda+2\mu+m)\frac{\partial u_1}{\partial Y}\frac{\partial^2 u_1}{\partial Y^2}+(4\mu+n)\frac{\partial u_1}{\partial Y}\frac{\partial^2 u_1}{\partial Z^2}\right)=0, \tag{2.17}$$

$$\frac{1}{4}k^2\left((4\lambda+4\mu+4m-n)\frac{\partial u_1}{\partial Y}\frac{\partial^2 u_1}{\partial Y\,\partial Z}+4(\lambda+2\mu+m)\frac{\partial u_1}{\partial Z}\frac{\partial^2 u_1}{\partial Z^2}+(4\mu+n)\frac{\partial^2 u_1}{\partial Y^2}\frac{\partial u_1}{\partial Z}\right)=0. \tag{2.18}$$

We apply displacement and force boundary conditions in solving these equations, as shown below.

#### 2.3.1. Application of displacement boundary conditions

The first- and second-order displacements are solved from the governing equations with displacement boundary conditions. The linear displacement $u_1$ can be solved from Eqs. (2.15), (2.17) and (2.18) as

$$u_1=\alpha_1 Y+\alpha_2 Z, \tag{2.19}$$

where $\alpha_1$ and $\alpha_2$ are constants. This solution represents simple shear in the first-order theory. Assuming that $u_1$ is a symmetric function of $Z$, we retain only the $Y$ dependence so that $u_1=\alpha Y$ with the linear shear strain $\alpha$ a constant. $\alpha$ can be determined from prescribed linear displacements at the top and bottom faces, i.e., $u_1(L_Y,Z)=\alpha L_Y$ and $u_1(0,Z)=0$ so that $\alpha=u_1(L_Y,Z)/L_Y$. For the nonlinear displacement $u_2$, it can be solved from the Laplace Equation Eq. (2.16) with the following boundary conditions on the bottom and top faces ($Y$=0, $L_Y$,):

$$u_2(0,Z)=0, \tag{2.20}$$

$$u_2(L_Y,Z)=g(Z), \tag{2.21}$$

i.e., the bottom face is fixed and $g(Z)$ is the nonlinear shear deformation prescribed at the top $Y=L_Y$. Furthermore, we define

$$u_2(Y,0)=u_2(Y,L_Z)=f(Y), \tag{2.22}$$

where $f(Y)$ is the nonlinear deformation of the block at $Z=0$ and $L_Z$, respectively; The shape $f(Y)$, which illustrates how the block deflects in the $X$–$Y$ plane, will be predicted. The second-order displacement $u_2$ can then be obtained as:

$$u_2(Y,Z)=\sum_{j=1}^{\infty}A_j\sin\left(\frac{j\pi Y}{L_Y}\right)\sinh\left(\frac{j\pi(L_Z-Z)}{L_Y}\right)+\sum_{j=1}^{\infty}B_j\sin\left(\frac{j\pi Y}{L_Y}\right)\sinh\left(\frac{j\pi Z}{L_Y}\right)+\sum_{j=1}^{\infty}D_j\sinh\left(\frac{j\pi Y}{L_Z}\right)\sin\left(\frac{j\pi Z}{L_Z}\right), \tag{2.23}$$

where

$$A_j = B_j = \frac{2}{L_Y \sinh(j\pi L_Z/L_Y)} \int_0^{L_Y} f(Y) \sin\left(\frac{j\pi Y}{L_Y}\right) dY, \tag{2.24}$$

and

$$D_j = \frac{2}{L_Z \sinh(j\pi L_Y/L_Z)} \int_0^{L_Z} g(Z) \sin\left(\frac{j\pi Z}{L_Z}\right) dZ. \tag{2.25}$$

This solution is symmetric about $Z=L_Z/2$. The aim is to obtain $f(Y)$ for various prescribed top face displacements $g(Z)$. For a given $g(Z)$, the Fourier coefficients $D_j$ can be calculated directly via Eq. (2.25). The other coefficients $A_j$ can be solved via force and moment boundary conditions (see below). With $A_j$ determined, Eq. (2.24) is essentially an integral equation in the unknown $f(Y)$.

### 2.3.2. Application of force and moment boundary conditions

The particular force and moment boundary conditions to be considered depend on the problem to be solved. From the components of the first Piola–Kirchoff stress (symmetric for this case), which can be deduced from Eq. (2.8):

$$\mathbf{T} = \begin{pmatrix} \frac{1}{2}k^2\alpha^2(m+\lambda+2\mu) & k\alpha\mu + k^2\mu\frac{\partial u_2}{\partial Y} & k^2\mu\frac{\partial u_2}{\partial Z} \\ k\alpha\mu + k^2\mu\frac{\partial u_2}{\partial Y} & \frac{1}{2}k^2\alpha^2(m+\lambda+2\mu) & 0 \\ k^2\mu\frac{\partial u_2}{\partial Z} & 0 & \frac{1}{4}k^2\alpha^2(2m-n+2\lambda) \end{pmatrix}, \tag{2.26}$$

it can be seen that all the normal stresses and the shear stress $T_{xZ}$ are second-order whereas the shear stress $T_{xY}$ consists of both first- and second-order parts. The normal components can be positive or negative; for many biogels $m+\lambda+2\mu$ is positive (Wang and Wu, 2014), which corresponds to negative normal stresses (Janmey et al., 2007). These normal stresses are necessary for maintaining the deformation of the generalized shear. The stress $T_{xY}$ on the $Y$-faces (top and bottom) gives rise to resultant forces and moments, and so do $T_{xZ}$ on the $Z$-faces (front and back). The nonlinear displacement $u_2$, which appears as derivatives in $T_{xY}$ and $T_{xZ}$, can be derived for particular force and moment boundary conditions. To illustrate this, we consider the following set of boundary conditions:

(BC 1). The shear forces on the $Y$-faces (top and bottom) are $F_{xY}$, which corresponds to the prescribed displacements $u_1(0,Z), u_1(L_Y,Z)$ and $u_2(0,Z), u_2(L_Y,Z)$.
(BC 2). No shear forces are applied on the $Z$-faces (front and back).
(BC 3). The moments prescribed on the $Z$-faces are $M_{xZ}$.

Moments may exist because of the existence of second-order shear stresses. Mathematically, the above boundary conditions can be written as:

$$\int T_{xY}\, dX\, dZ = F_{xY}, \quad \text{on } Z = 0, L_Z; \tag{2.27}$$

$$\int T_{xZ}\, dX\, dY = F_{xZ}, \quad \text{on } Z = 0,\ L_Z; \tag{2.28}$$

$$\int T_{xZ}(Z=0) Y\, dX\, dY - \int T_{xZ}(Z=L_Z) Y\, dX\, dY = M_{xZ}, \quad \text{on } Z = 0,\ L_Z. \tag{2.29}$$

The existence of $M_{xZ}$ (which is not identically zero) implies that a constraint against rotation about the $Z$-axis exists. In the experiments we carried out, rotation about the $Z$-axis was prevented, thus inducing a moment about that axis. This is analogous to the Poynting effect, in which the block expands or contracts under simple shear (equivalently a cylinder extends or shortens under torsion); otherwise if the block is constrained it will experience a normal stress. We note that the effect associated with $M_{xZ}$ does not exist under simple shear, for which $T_{xZ}$ does not exist.

Using the displacement expressions of Eq. (2.23) to evaluate the stresses of Eq. (2.26), and substituting the resulting stresses into Eqs. (2.27)–(2.29) yields

$$\int T_{xY}\, dX\, dZ = \left\{ \begin{array}{l} k\alpha\mu L_X L_Z + k^2\mu \sum_{j=1}^{\infty} L_X \left[ 2A_j \left( -1 + \cosh\left(\frac{j\pi L_Z}{L_Y}\right)\right) + D_j(1-(-1)^j)\right] = F_{xY}, \quad (Y=0) \\ k\alpha\mu L_X L_Z + k^2\mu \sum_{j=1}^{\infty} L_X \left[ 2A_j(-1)^j \left( -1 + \cosh\left(\frac{j\pi L_Z}{L_Y}\right)\right) + D_j(1-(-1)^j)\cosh\left(\frac{j\pi L_Y}{L_Z}\right)\right] = F_{xY}, \quad (Y=L_Y) \end{array} \right\}, \tag{2.30}$$

$$\int T_{xZ}\,dX\,dY=\left\{\begin{array}{ll} k^2\mu\sum\limits_{j=1}^{\infty}L_X\left[(-1+(-1)^j)A_j\left(\cosh\left(\frac{j\pi L_Z}{L_Y}\right)-1\right)+D_j\left(-1+\cosh\left(\frac{j\pi L_Y}{L_Z}\right)\right)\right]=0, & (Z=0)\\ k^2\mu\sum\limits_{j=1}^{\infty}L_X\left[(-1+(-1)^j)A_j\left(1-\cosh\left(\frac{j\pi L_Z}{L_Y}\right)\right)+D_j(-1)^j\left(-1+\cosh\left(\frac{j\pi L_Y}{L_Z}\right)\right)\right]=0, & (Z=L_Z)\end{array}\right\}, \tag{2.31}$$

$$\int T_{xZ}(Z=0)Y\,dX\,dY-\int T_{xZ}(Z=L_Z)Y\,dX\,dY$$
$$=k^2\mu\left(2\sum_{j=1}^{\infty}A_jL_XL_Y(-1)^j\left(\cosh\frac{j\pi L_Z}{L_Y}-1\right)-\sum_{j=1}^{\infty}\frac{L_X}{j\pi}D_j\left(-j\pi L_Y\cos\frac{j\pi L_Y}{L_Z}+L_Z\sin\frac{j\pi L_Y}{L_Z}\right)(\cosh(j\pi)-1)\right)=M_{xZ}, \tag{2.32}$$

where $A_j$ and $D_j$ are given in Eqs. (2.24) and (2.25). It can be seen that $F_{xY}$ in Eq. (2.30) contains both linear ($k$) and nonlinear terms ($k^2$). Hence, we take $F_{xY}=kF_1+k^2F_2$. Eqs. (2.30) and (2.31) can be written out, after some elementary rearrangement, as the following four equations:

$$k\alpha\mu L_XL_Z+k^2\mu L_X\sum_{j=1,3,5}^{\infty}\left[2A_j\left(-1+\cosh\left(\frac{j\pi L_Z}{L_Y}\right)\right)+2D_j\right]+k^2\mu L_X\sum_{j=2,4,6}^{\infty}\left[2A_j\left(-1+\cosh\left(\frac{j\pi L_Z}{L_Y}\right)\right)\right]=kF_1+k^2F_2 \tag{2.33}$$

$$k\alpha\mu L_XL_Z+k^2\mu L_X\sum_{j=1,3,5}^{\infty}\left[-2A_j\left(-1+\cosh\left(\frac{j\pi L_Z}{L_Y}\right)\right)+2D_j\cosh\left(\frac{j\pi L_Y}{L_Z}\right)\right]$$
$$+k^2\mu L_X\sum_{j=2,4,6}^{\infty}\left[2A_j\left(-1+\cosh\left(\frac{j\pi L_Z}{L_Y}\right)\right)\right]=kF_1+k^2F_2, \tag{2.34}$$

$$k^2\mu L_X\sum_{j=1,3,5}^{\infty}2A_j\left(\cosh\left(\frac{j\pi L_Z}{L_Y}\right)-1\right)=k^2\mu L_X\sum_{j=1,3,5}^{\infty}D_j\left(\cosh\left(\frac{j\pi L_Y}{L_Z}\right)-1\right), \tag{2.35}$$

$$k^2\mu\sum_{j=2,4,6}^{\infty}L_X\left[D_j\left(-1+\cosh\left(\frac{j\pi L_Y}{L_Z}\right)\right)\right]=0. \tag{2.36}$$

From Eq. (2.36), which involves summation over even values of $n$, it can be seen that $D_j=0$. Eq. (2.25) then shows that $g(Z)$ must be symmetric to $Z=L_Z/2$. As we restrict our study to symmetric prescribed displacement, we restrict to the case of $D_j=0$ for $n$ even. Substituting the above Eq. (2.35) into Eqs. (2.33) and (2.34) leads to the same equation with its linear and nonlinear parts shown below:

$$kF_1=k\alpha\mu L_XL_Z=k\mu u_1(L_Y,Z)L_XL_Z/L_Y, \tag{2.37}$$

$$k^2\left(F_2-\mu L_X\sum_{j=1,3,5}^{\infty}D_j\left(\cosh\frac{j\pi L_Y}{L_Z}+1\right)\right)=k^2\mu L_X\sum_{j=2,4,6}^{\infty}\left[2A_j\left(-1+\cosh\left(\frac{j\pi L_Z}{L_Y}\right)\right)\right]. \tag{2.38}$$

It can be seen that Eq. (2.37) is the solution for simple linear shear, in which the strain $\alpha$ is proportional to the stress $F_1/L_XL_Z$with the coefficient of shear modulus $\mu$. From Eqs. (2.32), (2.35) and (2.38), $F_2$ can be solved in terms of the prescribed $M_{xZ}$ and $D_j$ (known from prescribed displacement, see Eq. (2.25)):

$$F_2=\frac{M_{xZ}}{L_Y}+\mu L_X\sum_{j=1,3,5}^{\infty}\left(D_j\cosh\frac{j\pi L_Y}{L_Z}\right)+\sum_{j=1}^{\infty}\frac{\mu L_X}{j\pi L_Y}D_j\left(-j\pi L_Y\cos\frac{j\pi L_Y}{L_Z}+L_Z\sin\frac{j\pi L_Y}{L_Z}\right)(\cosh(j\pi)-1). \tag{2.39}$$

$A_j$ for $j$ odd and even can be determined separately from Eqs. (2.35) and (2.38). When $j$ is odd, if Eq. (2.35) is satisfied for every $j$, then $A_j$ can be derived as:

$$A_j=\frac{D_j(\cosh(j\pi L_Y/L_Z)-1)}{2(\cosh(j\pi L_Z/L_Y)-1)}. \tag{2.40}$$

When $j$ is even, Eq. (2.38) can be used to determine $A_j$. $A_j$ will be determined in next section.

Using the orthogonality of sine functions, Eq. (2.24) can be inverted to yield:

$$f(Y)=\sum_{j=1}^{\infty}A_j\sinh\frac{j\pi L_Z}{L_Y}\sin\frac{j\pi Y}{L_Y}=\sum_{j=1,3,5}^{\infty}A_j\sinh\frac{j\pi L_Z}{L_Y}\sin\frac{j\pi Y}{L_Y}+\sum_{j=2,4,6}^{\infty}A_j\sinh\frac{j\pi L_Z}{L_Y}\sin\frac{j\pi Y}{L_Y}. \tag{2.41}$$

It can be seen that $f(Y)$, which gives the shape of the block when viewed along the $Z$-direction, is a superposition of sine curves. Substituting Eq. (2.40) into Eq. (2.23), $u_2$ can be obtained. Thus the shear displacement $U$ can be written as:

$$U=u_1(Y)+u_2(Y,Z)=\alpha Y+\sum_{j=1,3,5}^{\infty}\left(\frac{D_j(\cosh(j\pi L_Y/L_Z)-1)}{2((\cosh j\pi L_Z/L_Y)-1)}(\sin(j\pi Y/L_Y)\sinh(j\pi(L_Z-Z)/L_Y)+\sin(j\pi Y/L_Y)\sinh(j\pi Z/L_Y))\right)$$
$$+\sum_{j=1,3,5}^{\infty}(D_j\sinh(j\pi Y/L_Z)\sin(j\pi Z/L_Z))+\sum_{j=2,4,6}^{\infty}A_j(\sin(j\pi Y/L_Y)\sinh(j\pi(L_Z-Z)/L_Y)+\sin(j\pi Y/L_Y)\sinh(j\pi Z/L_Y)). \tag{2.42}$$

In order to calculate $A_j$, $g(Z)$ should be given. Different shear displacements $g(Z)$ are considered next.

### 2.4. Solutions to particular problems

In this section, various shear displacements in the $X$-direction at the top face of the block are imposed. The prescribed displacement $U(L_Y, Z)$ is the sum of a linear part and a nonlinear part, i.e., $U(L_Y, Z) = u_1(L_Y) + u_2(L_Y, Z) = u_1(L_Y) + g(Z)$. Different constant values of $u_1(L_Y)$ and different functions $g(Z)$ can be prescribed. Three different forms of $g(Z)$ are chosen, as represented by constant, quadratic and sine functions. The generalization to a non-constant $g(Z)$ allows for the possibility of a more complex boundary condition, e.g., constraints to the edges of the top face of the block may prevent a uniform displacement. In the experiment study, however, we chose a constant $g(Z)$ for simplicity. For these three functions, the lateral profile $f(Y)$ and the total displacement $U(Y, Z)$ everywhere in the block are derived in the three subsections to follow.

#### 2.4.1. Constant shear displacement

In the first problem, $g(Z)$ is chosen as $g(Z) = \beta$, where $\beta$ is a constant. Substituting $g(Z) = \beta$ into Eq. (2.25), $D_j$ can be obtained as:

$$D_j = \frac{2\beta}{j\pi \sinh(j\pi L_Y/L_Z)}(1-(-1)^j). \tag{2.43}$$

Substituting Eq. (2.43) into Eq. (2.38) yields

$$\mu L_X \sum_{j=2,4,6}^{\infty} [2A_j(-1+\cosh(j\pi L_Z/L_Y))] = F_2 - \mu L_X \sum_{j=1,3,5,\ldots}^{\infty} \frac{4\beta}{j\pi}\frac{(1+\cosh(j\pi L_Y/L_Z))}{\sinh(j\pi L_Y/L_Z)}. \tag{2.44}$$

Since $\lim_{j\to\infty}(1+\cosh(j\pi L_Y/L_Z))/\sinh(j\pi L_Y/L_Z) = 1$ and $\sum_{j=1,3,5,\ldots}^{\infty} 1/j$ does not converge, Eq. (2.44) does not converge, unless $\beta = 0$. Thus, $\beta = 0$, which implies that in the second-order model we cannot prescribe a constant nonlinear displacement on the top face. Also, Eq. (2.43) shows that $D_j = 0$ for $j$ both odd and even.

Next, consider $j$ odd. Eq. (2.40) then becomes

$$A_j = \frac{D_j(\cosh(j\pi L_Y/L_Z)-1)}{2((\cosh j\pi L_Z/L_Y)-1)} = 0. \tag{2.45}$$

Since $A_j = 0$ for $j$ odd, $f(Y)$ consists of only even terms, and from Eq. (2.41)

$$f(Y) = \sum_{j=1}^{\infty} A_j \sinh\frac{j\pi L_Z}{L_Y}\sin\frac{j\pi Y}{L_Y} = \sum_{j=2,4,6}^{\infty} A_j \sinh\frac{j\pi L_Z}{L_Y}\sin\frac{j\pi Y}{L_Y}. \tag{2.46}$$

In principle, $A_j$ can be determined from minimization of the strain energy of the block subject to the constraint Eq. (2.38). $A_j$ decreases rapidly with $j$ because of the presence of the hyperbolic sine term in Eq. (2.46). On the other hand, our experimental results show that the second-order displacement of the side of the block is approximated well by a complete one-period sine curve. Hence, we choose $A_j = 0,\ j \neq 2$, and $A_2$ can then be solved from Eq. (2.38) as:

$$A_2 = \frac{F_2 - \mu L_X \sum_{j=1,3,5}^{\infty} D_j(\cosh(j\pi L_Y/L_Z)+1)}{2\mu L_X(\cosh(2\pi L_Z/L_Y)-1)}, \tag{2.47}$$

which, since $D_j = 0$, reduces to

$$A_2 = \frac{F_2}{2\mu L_X(\cosh(2\pi L_Z/L_Y)-1)}. \tag{2.48}$$

The force $F_2$ is determined from Eq. (2.39) as:

$$F_2 = \frac{M_{xZ}}{L_Y}. \tag{2.49}$$

The final form of $f(Y)$ is thus:

$$f(Y) = \frac{M_{xZ}}{2\mu L_X L_Y((\cosh 2\pi L_Z/L_Y)-1)}\sinh\frac{2\pi L_Z}{L_Y}\sin\frac{2\pi Y}{L_Y}, \tag{2.50}$$

and the total shear displacement in Eq. (2.42) becomes

$$U = u_1(Y) + u_2(Y,Z) = \frac{u_1(L_Y)}{L_Y}Y + \frac{M_{xZ}}{2\mu L_X L_Y((\cosh 2\pi L_Z/L_Y)-1)}\left(\sinh\frac{2\pi(L_Z-Z)}{L_Y} + \sinh\frac{2\pi Z}{L_Y}\right)\sin\frac{2\pi Y}{L_Y}. \tag{2.51}$$

The above result is a second-order solution for a block subjected to a prescribed constant top face displacement $u_1(L_Y)+\beta = u_1(L_Y)$ and a prescribed constant moment $M_{xZ}$ about the $Z$-axis. For these boundary conditions, the lateral profile is a sine curve (nonlinear shear displacement) superimposed on a straight line (linear shear displacement). There is also a hyperbolic sine dependence on $Z$ even though the prescribed displacement is uniform at the top face. This is a consequence of the requirement of the equilibrium equation which reduces to the Laplace equation.

*2.4.2. Parabolic shear displacement*

In the second problem, $g(Z)$ is chosen as $g(Z)=\gamma Z(L_Z-Z)/L_Z$, where $\gamma$ is an arbitrary constant. This is a parabolic profile, symmetric about $Z=L_Z/2$. $D_j$ can be obtained using Eq. (2.25) as:

$$D_j=\frac{4\gamma L_Z}{j^3\pi^3\sinh(j\pi L_Y/L_Z)}(1-(-1)^j). \tag{2.52}$$

Using Eqs. (2.52), (2.40) becomes, for $j$ odd

$$A_j=\frac{D_j(\cosh(j\pi L_Y/L_Z)-1)}{2(\cosh(j\pi L_Z/L_Y)-1)}=\frac{4\gamma L_Z}{j^3\pi^3\sinh(j\pi L_Y/L_Z)}\frac{(\cosh(j\pi L_Y/L_Z)-1)}{(\cosh(j\pi L_Z/L_Y)-1)}. \tag{2.53}$$

For $j$ even, $A_j$ should satisfy Eq. (2.38). The form of $f(Y)$, from Eq. (2.41), is thus

$$f(Y)=\sum_{j=1,3,5}^{\infty}\left(\frac{4\gamma L_Z}{j^3\pi^3\sinh(j\pi L_Y/L_Z)}\frac{(\cosh(j\pi L_Y/L_Z)-1)}{(\cosh(j\pi L_Z/L_Y)-1)}\sinh\frac{j\pi L_Z}{L_Y}\sin\frac{j\pi Y}{L_Y}\right)+\sum_{j=2,4,6}^{\infty}A_j\sinh\frac{j\pi L_Z}{L_Y}\sin\frac{j\pi Y}{L_Y}. \tag{2.54}$$

The total shear displacement $U$ can be obtained by substituting the corresponding $D_j$ and $A_j$ into Eq. (2.42). The form of Eq. (2.54), which satisfies the equilibrium equation, shows that $f(Y)$ is in general a superposition of harmonics. The first part on the right-hand side of Eq. (2.54) can be summed numerically over odd values of $j$ until convergence is reached. For the second part, it may only be necessary to sum over a finite number of even terms, and the values of $A_j$ can be determined by comparing with the experimental profile, subject to the constraint of Eq. (2.38).

*2.4.3. Sinusoidal shear displacement*

In the final problem, $g(Z)$ is chosen as $g(Z)=\gamma\sin\pi Z/L_Z$, where $\gamma$ is an arbitrary constant. $D_j$ can be obtained using Eq. (2.25) as:

$$D_1=\frac{\gamma}{\sinh(\pi L_Y/L_Z)},\quad D_j=0\ (j\neq 1). \tag{2.55}$$

Substituting the above $D_j$ into Eq. (2.40), $A_j$ for $j=1$ can be obtained as:

$$A_1=\frac{D_1(\cosh(\pi L_Y/L_Z)-1)}{2(\cosh(\pi L_Z/L_Y)-1)}=\frac{\gamma(\cosh(\pi L_Y/L_Z)-1)}{2(\cosh(\pi L_Z/L_Y)-1)\sinh(\pi L_Y/L_Z)}, \tag{2.56}$$

with $A_3$, $A_5$, $A_7$, etc. all equal to zero. For $j$ even, $A_j$ should satisfy Eq. (2.38). The form of $f(Y)$ can be obtained from Eq. (2.41) as

$$f(Y)=\frac{\gamma(\cosh(\pi L_Y/L_Z)-1)}{2(\cosh(\pi L_Z/L_Y)-1)\sinh(\pi L_Y/L_Z)}\sinh\frac{\pi L_Z}{L_Y}\sin\frac{\pi Y}{L_Y}+\sum_{j=2,4,6}^{\infty}A_j\sinh\frac{j\pi L_Z}{L_Y}\sin\frac{j\pi Y}{L_Y}. \tag{2.57}$$

As for the other cases, the total shear displacement $U$ can be obtained by substituting the corresponding $D_j$ and $A_j$ into Eq. (2.42).

*2.5. Solutions for generalized shear with gravity*

In this section, the solutions of a rectangular block subjected to a constant shear displacement $\delta$ on the top face in the presence of gravity $g$ are presented. The equilibrium equations are given by Eqs. (2.10)–(2.14). Specifically, Eq. (2.11) for $u_2$ reduces to a Poisson equation, instead of a Laplace equation. The solutions can be obtained by solving Eqs. (2.10)–(2.14) with the following boundary conditions:

(BC 1). The prescribed displacements on the $Y$-faces (top and bottom) are $\delta$ and zero respectively.
(BC 2). No shear forces are applied on the $Z$-faces (front and back).
(BC 3). The moments prescribed on the $Z$-faces are $M_{xZ}$.

Using similar procedures, it can be shown that the lateral profile $f(Y)$ can be written as

$$f(Y)=\frac{M_{xZ}}{2\mu L_X L_Y((\cosh 2\pi L_Z/L_Y)-1)}\sinh\frac{2\pi L_Z}{L_Y}\sin\frac{2\pi Y}{L_Y}-\frac{\alpha g\rho_0(\lambda+2\mu+m)}{2(\lambda+2\mu)\mu}Y^2, \tag{2.58}$$

where the linear shear strain $\alpha$ is

$$\alpha=\frac{\delta}{L_Y-((\rho_0 g(\lambda+2\mu+m))/(2(\lambda+2\mu)\mu))L_Y^2}. \tag{2.59}$$

The total shear displacement $U$ is

$$U=\alpha Y+\frac{M_{xZ}}{2\mu L_X L_Y(\cosh(2\pi L_Z/L_Y))-1}\left(\sinh\frac{2\pi(L_Z-Z)}{L_Y}+\sinh\frac{2\pi Z}{L_Y}\right)\sin\frac{2\pi Y}{L_Y}-\frac{\alpha g\rho_0(\lambda+2\mu+m)}{2(\lambda+2\mu)\mu}Y^2, \tag{2.60}$$

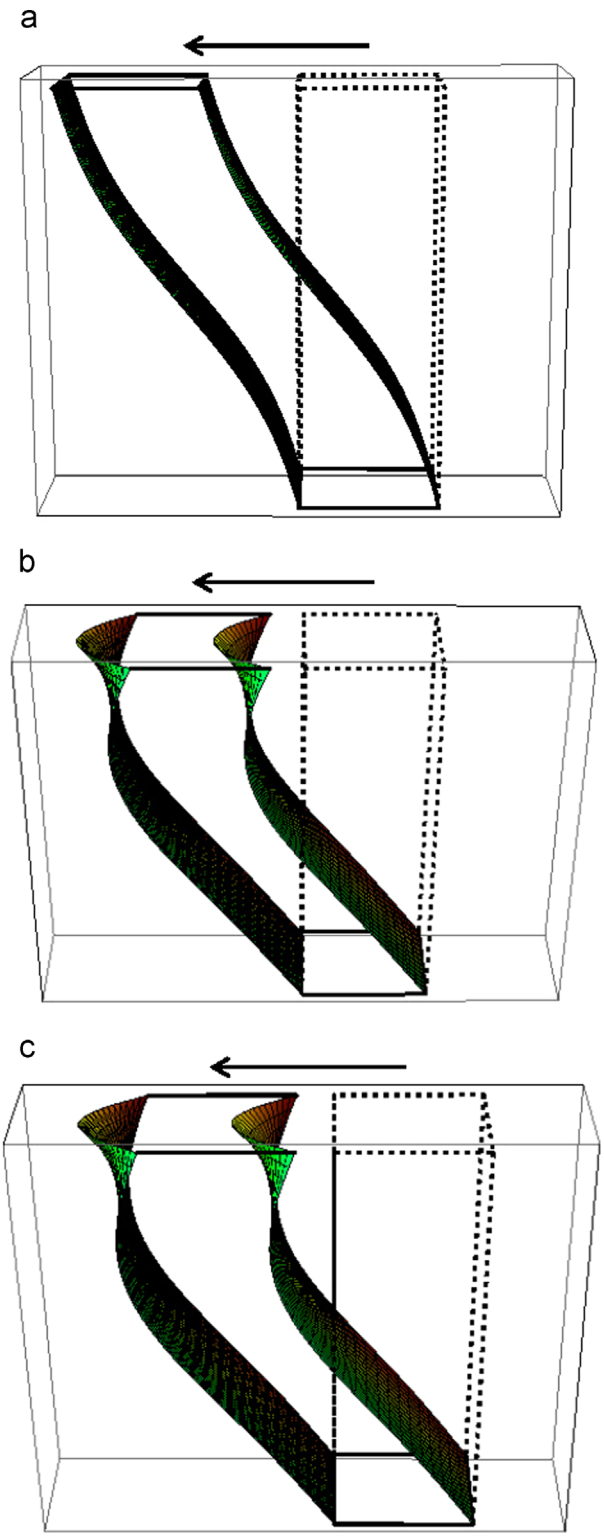


**Fig. 2.** Deformed and undeformed states for a rectangular block under generalized shear. The prescribed nonlinear displacement $g(Z)$ at the top face is assumed to be (a) constant, (b) quadratic, and (c) sinusoidal. The maximum shear displacements at the top and the applied moments $M_{xZ}$ on the $Z=0, L_Z$ faces are the same in all three cases.

By comparing Eqs. (2.58) and (2.60) with Eqs. (2.50) and (2.51), it can be seen that gravity has an additional effect, represented by $-\alpha g\rho_0(\lambda+2\mu+m)Y^2/2(\lambda+2\mu)\mu$, on the lateral profile and the shear displacement. The lateral profile takes the form of a straight line superimposed by a sine curve and a parabolic curve. In contrast, Destrade and Saccomandi (2010) showed that under gravity the lateral profile is a straight line superimposed by a parabolic curve only. This difference arises because we have taken $U$ to be a function of both $Y$ and $Z$ whereas they have taken it to be a function of $Y$ only.

## 3. Numerical examples and experiments

In this section, we illustrate the key findings of the paper through numerical examples. Specifically, we show that if gravity is neglected: (a) the nonlinear displacement within the block can be described by the superposition of the products of hyperbolic sine functions of the depth $Z$ and sine functions of the height $Y$, (b) the lateral profile of the deformed block under shear can be described by the superposition of a straight line and a complete (one-period) sine curve, (c) an out-of-plane shear stress $T_{xZ}$ is induced, which further distorts the block, and (d) normal stresses are also induced, which demonstrates the Poynting effect or the dilation/shrinking of the block. Simple experiments have also been conducted to show that the lateral profile is well-approximated by theory.

### 3.1. Theoretical predictions of the shape of the deformed block

Fig. 2(a)–(c) show the predicted shapes of a block when subjected to three different prescribed shear displacements on $Y=L_Y$: constant, parabolic and sinusoidal, respectively. For all three cases, the block dimensions are $L_X=0.024$ m, $L_Y=0.072$ m and $L_Z=0.020$ m, and the prescribed moment $M_{xZ}/\mu=-7.29\times10^{-6}$ m$^3$. The prescribed displacements for Fig. 2(a)-(c) are given by $u_1(L_Y)=0.04$ m and $g(Z)=0$, $u_1(L_Y)=0.03$ m and $g(Z)=2Z\ (L_Z-Z)/L_Z$, and $u_1(L_Y)=0.03$ m and $g(Z)=0.01\sin(\pi Z/L_Z)$, respectively. The maximum shear displacements in all three cases equal 0.04 m. All the results are generated with $A_4=A_6=\ldots..=0$, with $A_2$ calculated from $M_{xZ}$ using Eqs. (2.38) and (2.39).

It can be seen that the deformed shapes are curved with respect to both the $X$–$Y$ and $X$–$Z$ planes, including that under a constant prescribed shear displacement, although the curvature is not that obvious in the $X$–$Z$ plane. The curvature in the $X$–$Z$ plane has its origin in the hyperbolic sine term, while that in the $X$–$Y$ plane reflects the sine term. The $\sin 2\pi Y/L_Y$ term results in a point of inflection in the lateral profile, which differs from what a $Y^2$ dependence would predict.

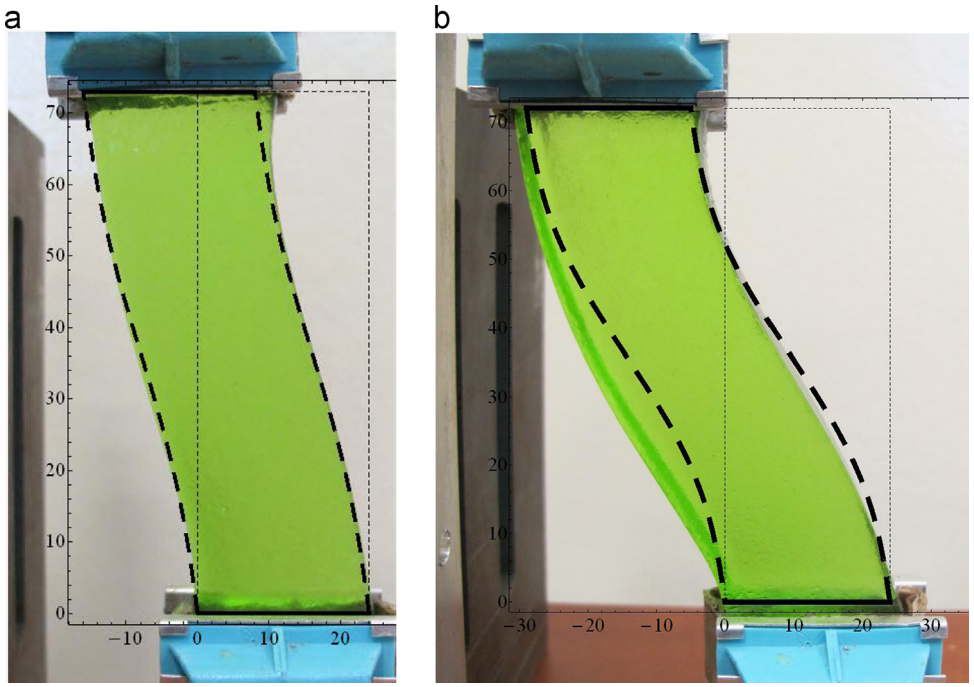


**Fig. 3.** Rectangular blocks of agar–gelatin gel, with $L_X=0.024$ m, $L_Y=0.072$ m, and $L_Z=0.014$ m, subjected to the constant shear displacement (a) 0.016 m and (b) 0.029 m at the top faces. Each block was gripped at the top and the bottom was sheared rightward. The theoretical lateral profiles are shown as dashed lines. Agreement between theory and experiments is good, with some noticeable discrepancy in the case of the larger prescribed shear.

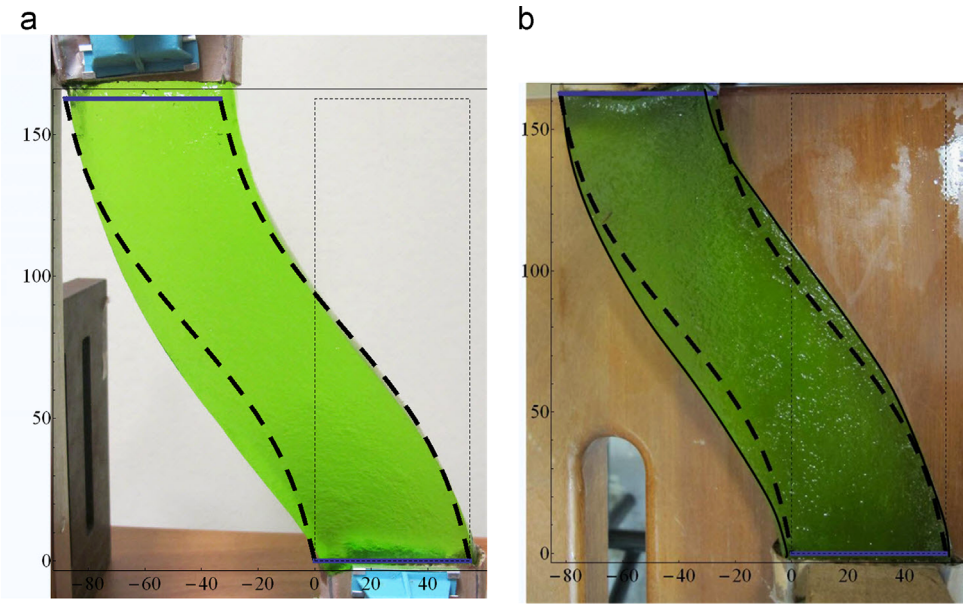


**Fig. 4.** Shear displacement of (a) vertically standing and (b) horizontally lying gels. The dashed lines are the theoretical predictions. The effect of gravity is highlighted in (a). However, significant nonlinearity and the Poynting effect may also have resulted in a discrepancy, as shown in (b), where gravity plays a minor role.

### 3.2. *Experimental and theoretical studies of the lateral profile of the deformed block*

To verify the lateral profile $f(Y)$, we carried some simple experiments using an edible agar–gelatin consumed as a dessert. This was easily made by dissolving different amounts of the powder in water, resulting in soft blocks of various densities. Figs. 3 and 4 show a gel made by dissolving 300 g of powder into 1.25 and 1 l of water, respectively. The experiments were carried out for a prescribed uniform shear: the bottom face was encased in a holder and moved rigidly to the right while holding the upper face in an immovable holder.

Fig. 3 compares the shapes of the block subjected to two different uniform shear displacements. The block dimensions are $L_X=0.024$ m, $L_Y=0.072$ m, $L_Z=0.014$ m. The prescribed total displacements are 0.016 m and 0.029 m, for Fig. 3(a) and (b), respectively. The lateral profiles are as shown in the photos contained in Fig. 3. They look similar to the predicted profile shown in Fig. 2(a), i.e., a superposition of a straight line and a complete sine curve with a point of inflection. The experimental lateral profiles were then fitted using our model without considering gravity, with the linear shear strain $\alpha=0.222$ for Fig. 3(a) and $\alpha=0.403$ for Fig. 3(b), calculated in each case by dividing the total shear displacement by the height of the block. The amplitudes of the sine curve, given by $A_2 \sinh(2\pi L_Z/L_Y)$, were estimated from the experimental profiles to be $A_2=0.65$ mm and 1.94 mm, respectively. The dotted lines show the theoretical predictions. It can be seen that the theoretical and experimental lateral profiles agree quite well for these rather large prescribed displacements. There is, however, some discrepancy in the case of the larger prescribed displacement. This may be attributed to three effects: (a) the inaccuracy of a second-order nonlinear elasticity model, (b) the additional displacements which arise because the block is not constrained to support the second-order normal stresses (Poynting effect), and (c) the gravity effect.

To demonstrate the influence of gravity, we carried out experiments with very long gels, with some blocks standing vertically as before and with others lying flat on a surface. For the latter, gravity should have little effect on their lateral profiles. Fig. 4 shows two typical examples for an agar–gelatin with $L_X=0.055$ m, $L_Y=0.163$ m, $L_Z=0.025$ m. The prescribed shear displacements are 0.088 and 0.082 m, respectively for Fig. 4(a) and (b). Also, $\alpha=0.54$ and 0.50, and $A_2=7.14$ mm for the two figures. The dotted lines show the theoretical predictions of the lateral profiles. There is greater discrepancy between theory and experiment when the block is standing up vertically than lying flat on the surface. This implies that gravity does have an effect on the deformed shape of the soft gel. However, the elastic nonlinearity and the Poynting effect may have an effect as well, as a discrepancy also exists when the block lies flat on its side; for this case gravity should play a much smaller role in the profile.

Fig. 5 plots the difference between the lateral profiles at $Y=L_Y/2$ predicted with and without gravity. This difference is given by $\Delta U = U_{\text{nogravity}}(L_Y/2, L_Z) - U_{\text{withgravity}}(L_Y/2, L_Z)$. The parameters used are $L_X=0.024$ m, $L_Y=0.072$ m, $L_Z=0.02$ m, $\alpha=0.08$, and $A_2=-1.44\times10^{-4}$ m. Fig. 5(a) and (b) plot $\Delta U$ versus $\mu$ for different values of $\nu$ and $m$, with $m=-50000$ Pa and $\nu=0.45$, respectively. In order to show the effect of the Poisson ratio $\nu$, $\lambda$ is replaced by $2\mu\nu/(1-2\nu)$. The figure shows that the difference is maximum when $\mu$ approaches zero and vanishes at large values of $\mu$ ($>400$ Pa, say), regardless of $m$ and $\nu$. On the other hand, Fig. 5 also shows that the difference is less important if the material is nearly incompressible or if $m$ has a small negative value such as $-1000$ Pa. Roughly speaking, $\Delta U$ lies in the range of $10^{-4}$–$10^{-3}$ m, which is one order

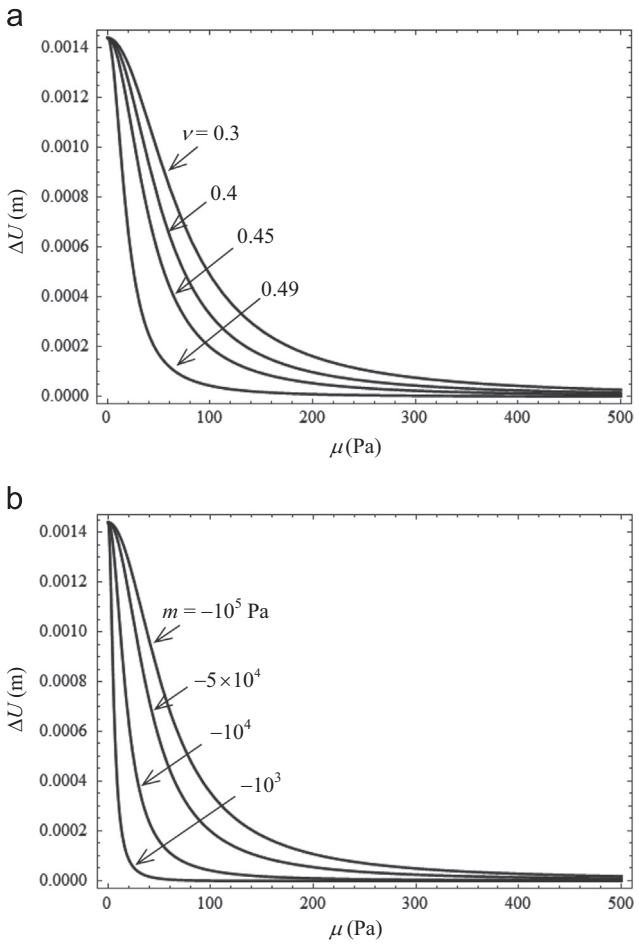


**Fig. 5.** Dependence of the difference $\Delta U$ between the lateral profiles at mid-height of a block considering and without considering gravity on the elastic constants. The block is subjected to a constant shear displacement of 5.76 mm at the top. (a) Dependence on $\mu$ and $\nu$, (b) dependence on $\mu$ and $m$. $\Delta U$ is larger at small $\mu$, small $\nu$ and large negative values of $m$.

of magnitude smaller than $L_X$. This implies that the gravity may play some role in the deformation of the block. In conclusion, the gravity effect becomes less significant for large $\mu$, large $\nu$ and small negative $m$.

### 3.3. *Investigation of the Poynting effect*

Janmey et al. (2007) have studied the relations between the applied shear strain and the Cauchy stress components $T_{xy}$ and $T_{yy}$ (the subscripts are in lower case) for various soft materials. Fig. 6(a) shows these relations for matrigel and polyacrylamide for shear strains of up to 100%. It can be seen that matrigel experiences a negative normal stress, whereas polyacrylamide a positive normal stress, implying that the two materials exhibit negative and positive Poynting effect, respectively.

According to Eq. (2.26), second-order normal stresses are also induced in the generalized shear. The first Piola Kirchoff stress $\mathbf{T}$ can be converted to the Cauchy stress $\mathbf{T}_C$ (with components denoted by $T_{xy}$, $T_{yy}$, etc.) using the formula $\mathbf{T}_C = (1/\det\mathbf{F})\mathbf{T}\mathbf{F}^*$, with $\det\mathbf{F}=1$. The Cauchy stress components *Txy* and *Tyy* are plotted in Fig. 6(b), with $\lambda=1350$, $\mu=150$, $m=-1000$ Pa for matrigel and $\lambda=585$, $\mu=65$, $m=-780$ Pa for polyacrylamide. Here we have also taken $A_2=A_4=\ldots=0$. Fig. 6(a) and (b) compares well qualitatively.

The experimental and theoretical results above show the dependence of the Poynting effect on the elastic parameters. Fig. 7(a) and (b) plot the variation of the stress ratio $T_{yy}/T_{xy}$ with the shear modulus $\mu$ for different values of Poisson's ratio $\nu$ and the third-order elastic constant $m$, respectively. In Fig. 7(a), where $m=-2000$ Pa, several results are noteworthy. First, the closer $\nu$ is to 0.5, the more likely the Poynting effect will be negative. For soft materials which are nearly incompressible, the negative Poynting effect may thus be prevalent. Second, $\mu$ also appears to have a significant influence. If $\mu > \sim 600$ Pa, a material with high or near incompressibility will experience a negative Poynting effect. If $\mu$ is very small, less than 100 Pa, say, then the Poynting effect is positive if $\nu$ is less than $\sim 0.47$. In Fig. 7(b), where $\nu=0.45$, the importance of $m$ is highlighted. It can be observed that for $m>0$, the negative Poynting effect is predicted regardless of the value of $\mu$, while for $m<0$,

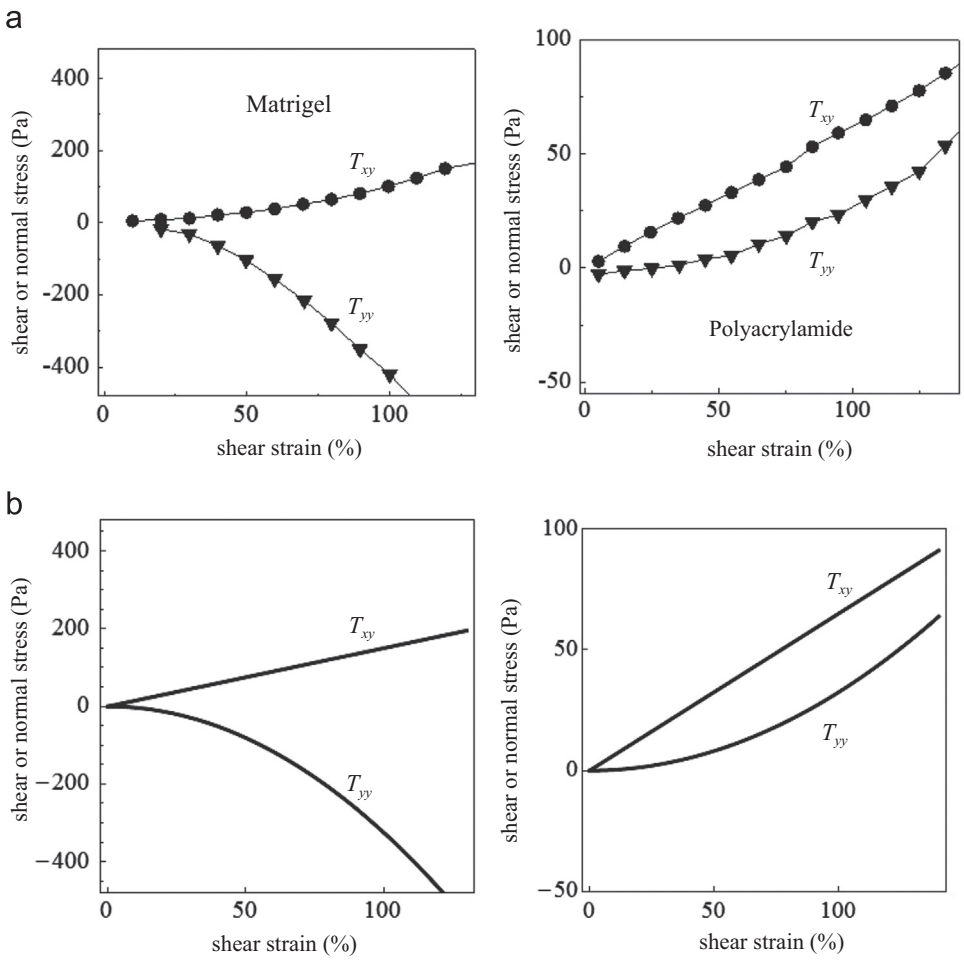


**Fig. 6.** Comparison of (a) experimental shear ($T_{xy}$) and normal ($T_{yy}$) stresses versus shear strain with (b) theoretical predictions. The gels were made from matrigel and polyacrylamide (Janmey et al., 2007). Negative and positive normal stresses were found to be present, and were also predicted by theory.

the effect depends on the value of $\mu$. For example, the positive Poynting effect is predicted for small $\mu$ in the case of $m<0$. The dependence of the Poynting effect on the second- and third-order elastic constants has been studied by the authors for the torsion of homogeneous and composite cylindrical bars in a previous paper (Wang and Wu, 2014).

### 3.4. Out-of-plane shear stress

A second-order out-of-plane shear stress $T_{xZ}$ arises in generalized shear when the nonlinear displacement $u_2$ is a function of both $Y$ and $Z$. This shear component distorts the lateral profile into a curve with an inflection point. In the second-order elasticity model, the profile is a superposition of a straight line with a complete sine curve, which well approximates our experimental results. Fig. 8(a) plots the ratio $T_{xZ}/T^L_{xY}$ versus the $Y$- and $Z$-coordinates, where the parameters are $L_X=0.024$ m, $L_Y=0.072$ m, $L_Z=0.02$ m, $\alpha=0.05$, and $A_2=-1.44\times10^{-4}$ m. $T_{xZ}$is of the same order of magnitude as $T^L_{xY}$, which is the in-plane shear stress corresponding to the linear shear strain $\alpha$. Hence, $T_{xZ}$ is not negligible. Similarly, the nonlinear component $T^{NL}_{xY}$ is also not negligible compared to $T^L_{xY}$. Fig. 8 shows that all the second-order shear stresses are generally of significant magnitude and play a fundamental role in the distortion of a soft block. Furthermore, Eq. (2.26) shows that the first- and second-order shear stresses are all proportional to $\mu$ and not to the other elastic constants.

## 4. Discussion

The essential difference between the current and previous works lies in the different deformation assumptions. The current work, which assumes that the second-order displacement $u_2$ is a function of both $Y$ and $Z$, is represented by Eq. (1.5). The other works assume that it is a function of $Y$ only, as shown in Eqs. (1.1)–(1.4). In the context of second-order elasticity, the equilibrium equation $k^2\mu(\partial^2u_2/\partial Y^2+\partial^2u_2/\partial Z^2)=0$, i.e., Eq. (2.16), predicts that $u_2$ can at most be a linear function of $Y$ if $u_2$ is a function of only $Y$. With a dependence on both variables, Eq. (2.16) is the Laplace equation and the solution takes the

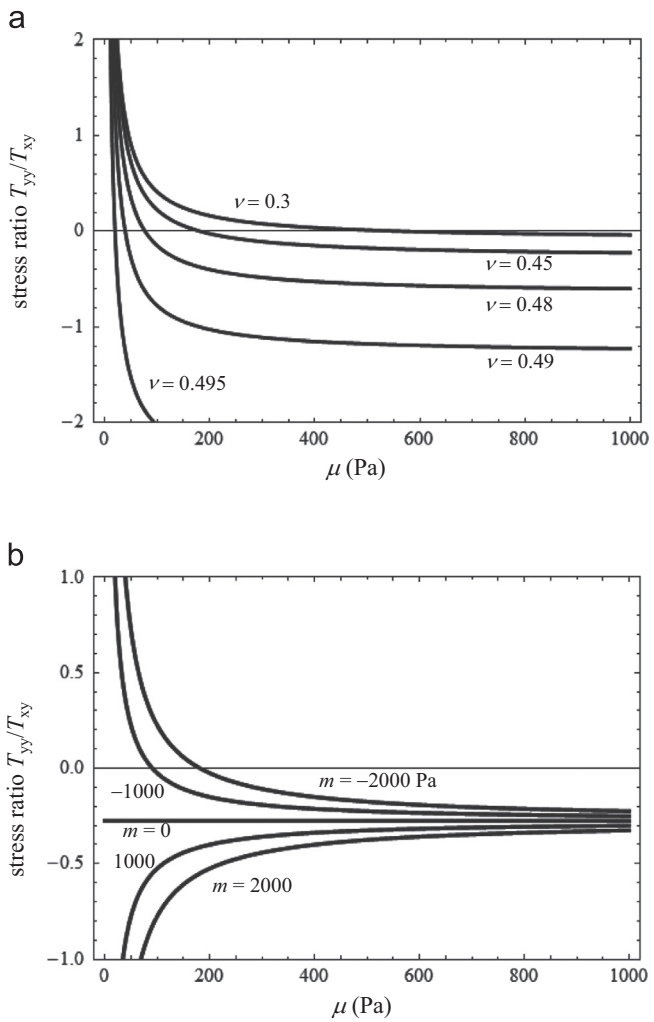


**Fig. 7.** (*a*) Dependence of the stress ratio $T_{yy}/T_{xy}$ with $\mu$ for different values of (a) $\nu$ between 0.3 and 0.495, and (b) $m$ between -2000 and 2000 Pa. The induced normal stress becomes important at small $\mu$, large $\nu$, and large positive or negative $m$.

form of the product of sine and hyperbolic sine functions. Experimentally, $u_2$ is not seen to be a linear function of $Y$ and hence the assumption of a dual dependence on $Y$ and $Z$ is justified. Furthermore, we can deduce from Eq. (2.16) that the assumption of $u_2 = Y^2$ does not satisfy the equilibrium equation. Hence, the validity of the assumption of a quadratic profile should be checked for other constitutive models. The general equation for the lateral profile, Eq. (2.41), shows that soft blocks which deform without a point of inflection over the height of the block can also be modeled, e.g., by the superposition of a straight line and a half sine curve. This profile would then resemble a quadratic one, and would also satisfy the equilibrium equation. In a more general sense, Eq. (2.41) is like a Fourier series, which can mathematically model any smooth curve.

The assumption of Eq. (1.5) also results in the existence of a second-order in-plane shear stress $T_{xY}^{NL}$ as well as a second-order out-of-plane shear stress $T_{xZ}$. These shear stresses are not predicted if the other deformation assumptions are made as in Eqs. (1.1)–(1.4). They may also be significant in magnitude, as shown in Fig. 8. $T_{xZ}$ is analogous to, but distinct from, the normal stresses which correspond to the Poynting effect. In other words, the Poynting effect exists under simple shear, and both $T_{xZ}$ and the Poynting effect exist under generalized shear. This implies that under generalized shear, a soft block will undergo (i) an in-plane shear, (ii) a stretching or contraction in the normal directions (positive or negative Poynting effect), and (iii) an out-of-plane shear tending to distort the block about the $Y$-axis. If the deformations in (ii) and (iii) are constrained, the corresponding normal and out-of-plane shear stresses will be induced.

In real physiological and engineering environments, biomaterials may experience generalized shear rather than simple shear because of the presence of multiaxial loads and constraints. For instance, $T_{xZ}$ distorting a cell under generalized shear may have a significant effect on the overall force balance in the cytoskeleton. It may also alter the structure of the cell, which is sensitive to the stresses it experiences. A case in point is the uni-directional shearing of blood cells, which however may

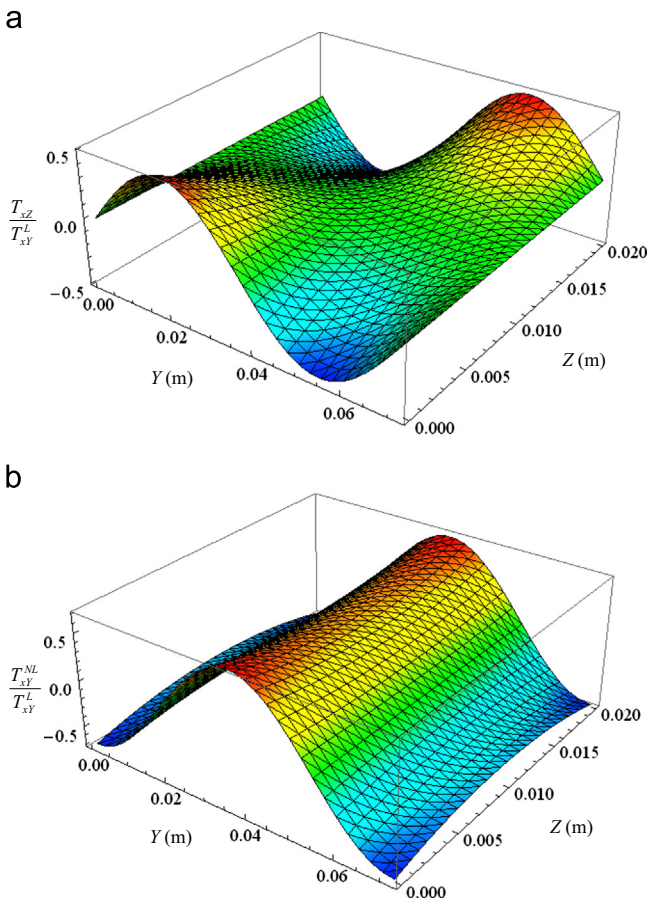


**Fig. 8.** Dependence of the ratio of the nonlinear to linear shear stress (*a*) $T_{xZ}/T^L_{xY}$ and (*b*) $T^{NL}_{xY}/T^L_{xY}$ on the $Y$ and $Z$ coordinates of a rectangular block under generalized constant shear. It can be observed that the nonlinear stresses are generally significant. Hence the simple shear model, which predicts $T_{xZ}/T^L_{xY}=0$, is inappropriate for soft gels, generally speaking.

experience shearing deformation in all three planes. The red blood cell may thus be deformed, damaged or undergo structural changes (Leverett et al., 1972; Meram et al., 2013).

Second, our results may have interesting implications in the design of actuators and sensors. A multi-plane actuator can be designed, based on the phenomenon that a soft material can undergo an out-of-plane distortion under generalized shear in one direction. The distortion of the plane may generate a moment, which can be used to actuate a connecting device. Similarly, a sensor can be designed to detect and measure the deformation in a plane which is orthogonal to the signal occurring in another plane.

The sign of the normal stresses shown in Eq. (2.26) can be explicitly used to judge the direction of the Poynting effect. Eq. (2.26) may also be used in a reverse manner to determinate the third-order elastic constants, assuming that the second-order constants $\lambda$ and $\mu$ have been determined by other means. A simple illustration is as follows. By measuring the $T_{yY}$ necessary to maintain a generalized shear deformation of a rectangular block, the elastic constant $m$ of the material can be estimated, as $T_{yY}$ is dependent on $\lambda$, $\mu$ and $m$. Next, the value of $n$ can be estimated by measuring $T_{zZ}$, which is dependent on $\lambda$, $m$ and $n$. As pointed out by Janmey et al. (2007) and predicted by our numerical results, the normal stresses can be as large as the shear stress. Thus, measuring the normal stresses may be a simple way to estimate the third-order elastic constants and provides an alternative to acousto-elastic methods (Catheline et al., 2003; Destrade et al., 2010).

Although this work considers second-order nonlinearity and generalized shear, it does not consider inhomogeneity, anisotropy, time-independent viscoelasticity, and higher-order nonlinearity. Many natural biomaterials are composites, architecturally hierarchical and exhibit time-dependent behavior. Nonlinearity can be investigated with higher-order elasticity models. The study of composite materials poses a significant challenge, which possibly can be met by adapting the method used in the present work. Anisotropy can also be incorporated, through the use of additional invariants in the strain energy density. Viscoelasticity adds considerable difficulty to the problem, which most likely requires numerical methods of solutions. A natural extension of our current work is to the problem of composite materials under generalized shear.

Finally, the existence and uniqueness of solutions in nonlinear elastic problems deserve a special mention here, as interpretations of nonlinear phenomena such as the Poynting effect would depend on these solutions. Green et al. (1952)

developed the general theory of small elastic deformations superposed on finite elastic deformations. The existence, uniqueness and analyticity of solutions for boundary value problems of nonlinear bodies were subsequently studied by various researchers, e.g., Hill (1957), Ball (1977), Ciarlet (1988), and Valent (1988). Valent (1988) proved a number of theorems which permitted the use of Signorini's method for solving pure traction-value problems of spheres and cylinders subjected to uniform pressure. In the work reported here, the nonlinear effects, as predicted within the second-order elasticity framework of Murnaghan (1951), depend on the elastic constants. The values of these constants were derived from experimental data of real materials. Generally speaking, an investigation of the dependence of the nonlinear effects on the elastic constants should be treated with caution, especially if the constants have not been measured directly, or if they have not been determined via fitting to the experimental data of the mechanical response.

## 5. Conclusions

This paper develops analytical solutions for a homogeneous rectangular block under generalized shear in the framework of second-order elasticity. The major contributions and findings can be summarized as follows.

Firstly, the analytical solutions show that the second-order shear displacements are characterized by the product of sine and hyperbolic sine functions of the height and depth variables, respectively. The solutions also reveal that the lateral profile is a straight line superimposed on sine curves under a prescribed constant shear displacement. This profile is verified by experiments.

Secondly, an out-of-plane nonlinear shear stress is generated under generalized shear, which may twist/distort the block about the height direction. This phenomenon may have implications in the design of biomaterials and bio-inspired materials..

Thirdly, nonlinearity is a significant part of the displacements and stresses for soft materials, e.g., the out-of-plane shear stress.

Fourthly, nonlinear normal stresses, which are related to the Poynting effect, are needed to maintain the deformation. The Poynting effect is significantly dependent on the elastic constants, e.g., $\nu$ and $m$. By measuring the normal stresses, third-order elastic constants can be estimated.

Finally, the effect of gravity has been investigated. Our results show that an extra quadratic term will arise in the dependence of the shear displacement on the height in the presence of gravity. The gravity effect becomes less significant for large $\mu$, large $\nu$ and small negative $m$.

## References


Ball, J.M., 1977. Convexity conditions and existence theorems in nonlinear elasticity. Arch. Ration. Mech. Anal. 63, 337–403.

Catheline, S., Gennisson, J.L., Fink, M., 2003. Measurement of elastic nonlinearity of soft solid with transient elastography. J. Acoust. Soc. Am. 114, 3087–3091.

Ciarlet, P.G., 1988. Mathematical Elasticity. Three-dimensional Elasticity, Elsevier Science Publishers B.V. vol. I; .

Destrade, M., Gilchrist, M.D., Ogden, R.W., 2010. Third- and fourth-order elasticities of biological soft tissues. J. Acoust. Soc. Am. 127, 2103–2106.

Destrade, M., Murphy, J.G., Saccomandi, G., 2012. Simple shear is not so simple. Int. J. Non-Linear Mech. 47, 210–214.

Destrade, M., Saccomandi, G., 2010. On the rectilinear shear of compressible and incompressible elastic slabs. Int. J. Eng. Sci. 48, 1202–1211.

Gardiner, J.C., Weiss, J.A., 2001. Simple shear testing of parallel-fibered planar soft tissues. ASME J. Biomech. Eng. 123, 170–175.

Green, A.E., Rivlin, R.S., Shield, R.T., 1952. General theory of small elastic deformations superposed on finite elastic deformations. Proc. R. Soc. Lond. A 211, 128–154.

Hill, R., 1957. On uniqueness and stability in the theory of finite elastic strain. J. Mech. Phys. Solids 5, 229–241.

Horgan, C.O., Murphy, J.G., 2011. Simple shearing of soft biological tissues. Proc. R. Soc. A – Math. Phys. 467, 760–777.

Janmey, P.A., Mccormick, M.E., Rammensee, S., Leight, J.L., Georges, P.C., Mackintosh, F.C., 2007. Negative normal stress in semiflexible biopolymer gels. Nat. Mater. 6, 48–51.

Kang, H., Wen, Q., Janmey, P.A., Tang, J.X., Conti, E., MacKintosh, F.C., 2009. Nonlinear elasticity of stiff filament networks: strain stiffening, negative normal stress, and filament alignment in fibrin gels. J. Phys. Chem. B 113, 3799–3805.

Leverett, L.B., Hellums, J.D., Alfrey, C.P., Lynch, E.C., 1972. Red blood cell damage by shear stress. Biophys. J. 12, 257–273.

Meram, E., Yilmaz, B.D., Bas, C., Atac, N., Yalcin, O., Meiselman, H.J., Baskurt, O.K., 2013. Shear stress-induced improvement of red blood cell deformability. Biorheology 50, 165–176.

Mihai, L.A., Goriely, A., 2011. Positive or negative Poynting effect? The role of adscititious inequalities in hyperelastic materials. Proc. R. Soc. A – Math. Phys. 467, 3633–3646.

Mihai, L.A., Goriely, A., 2013. Numerical simulation of shear and the Poynting effects by the finite element method: an application of the generalised empirical inequalities in non-linear elasticity. Int. J. Non-Linear Mech. 49, 1–14.

Misra, S., Ramesh, K.T., Okamura, A.M., 2010. Modelling of non-linear elastic tissues for surgical simulation. Comput. Methods Biomech. Biomed. Eng. 13, 811–818.

Murnaghan, F.D., 1951. Finite Deformation of an Elastic Solid. John Wiley, New York.

Poynting, J.H., 1909. On pressure perpendicular to the shear planes in finite pure shears, and on the lenghtening of loaded wires when twisted. Proc. R. Soc. Lond. A – Cont. A 82, 546–559.

Rivlin, R.S., 1948. Large elastic deformations of isotropic materials. IV. Further developments of the general theory. Philos. Trans. R. Soc. Lond. A 241, 379–397.

Storm, C., Pastore, J.J., MacKintosh, F.C., Lubensky, T.C., Janmey, P.A., 2005. Nonlinear elasticity in biological gels. Nature 435, 191–194.

Valent, T., 1988. Boundary Value Problems of Finite Elasticity. Springer Verlag, New York.

Wang, D., Wu, M., 2014. Poynting and axial force-twist effects in nonlinear elastic mono- and bi-layered cylinders: torsion, axial and combined loadings. Int. J. Solids Struct. 51, 1003–1019.

Wu, M.S., Kirchner, H.O.K., 2010. Nonlinear elasticity modeling of biogels. J. Mech. Phys. Solids 58, 300–310.